Journal of Applied Physics

Effect of shell permutation on electromagnetic properties of $ZnFeO_4$/(PANI, SiO_2) core/double-shell nanostructured disks

Cite as: J. Appl. Phys. **117**, 17A505 (2015); https://doi.org/10.1063/1.4918759
Submitted: 22 September 2014 . Accepted: 29 December 2014 . Published Online: 22 April 2015

Jiaheng Wang, Siu Wing Or, and Chung Ming Leung

Effect of shell permutation on electromagnetic properties of $ZnFeO_4$/(PANI, SiO_2) core/double-shell nanostructured disks

Jiaheng Wang, Siu Wing Or,[a] and Chung Ming Leung
Department of Electrical Engineering, The Hong Kong Polytechnic University, Hung Hom, Kowloon, Hong Kong

(Presented 7 November 2014; received 22 September 2014; accepted 29 December 2014; published online 22 April 2015)

$ZnFe_2O_4$/PANI/SiO_2 (ZPS) and $ZnFe_2O_4$/SiO_2/PANI (ZSP) core/double-shell nanostructured disks comprising PANI conducting dielectric shell and SiO_2 insulating dielectric shell on a disk-shaped $ZnFe_2O_4$ magnetic core are prepared to study the effect of shell permutation on their electromagnetic properties. The complex relative permittivity ($\varepsilon_r = \varepsilon_r' - j\varepsilon_r''$) and permeability ($\mu_r = \mu_r' - j\mu_r''$) of ZPS and ZSP are measured, and the reflection loss (*RL*) is determined, together with the $ZnFe_2O_4$ core, in the 1–18 GHz range. ε_r' and ε_r'' in ZPS and ZSP are smaller than the core because of the induction of disordered dipolar polarizations at various interfaces involving the insulating SiO_2 shell. Two obvious dielectric and magnetic abnormalities are observed in ZPS and ZSP. First, ε_r'' is weakened in the dipolar polarization-rich ZPS when compared to the ZSP of relatively less dipolar polarization. Second, μ_r' and μ_r'' in ZPS become the largest in the 1.5–10.8 and 5.6–18 GHz ranges, respectively, while μ_r'' in ZSP remains the lowest and changes to be negative in the 10–18 GHz range, among all samples. An electromagnetic energy transformation mechanism is proposed to explain the observed abnormalities and their effects on absorption. © *2015 AIP Publishing LLC*. [http://dx.doi.org/10.1063/1.4918759]

The incorporation of microwave absorbers in electromagnetic (EM) design has been recognized as an effective way to alleviate the problems of EM interference and pollution.[1] Advanced microwave absorbers based on magnetic/dielectric core/shell nanostructures have been a main research focus in recent years,[2–6] and research works have been directed to include conducting or insulating dielectric shells.[2–4] For the nanostructures using conducting dielectric shells (e.g., Ni/C, Ni/PANI, etc.), the enhancement of EM properties by increasing multiple dipolar polarizations and magnetic natural resonances has been widely observed.[2,3] For those involving insulating dielectric shells (e.g., Fe/SiO_2, Fe/PU, etc.), the weakening of EM properties by decreasing conductivity and saturation magnetization has been commonly found.[4] Nevertheless, the narrow absorbing bandwidth and large variation in absorption with absorber thickness intrinsic to the core/shell nanostructures have offered great challenges to further development and applications.[5,6]

Within these several years, magnetic/dielectric core/double-shell nanostructures have emerged as a highly prospective candidate for microwave absorbers because of their potentially improved designability and material availability enabled by the addition of the 2nd shell.[7,8] In fact, these core/double-shell nanostructures can be configured to simply own double-conducting or double-insulating dielectric shells, or to simultaneously own conducting and insulating dielectric shells. From a physical perspective, the distinct dielectric properties of the conducting and insulating dielectric shells will bring about characteristically different interfacial effects and, hence, EM properties in the nanostructures, especially for those configured with conducting and insulating dielectric double-shells. Therefore, the permutation of shells plays an important role in the development of magnetic/dielectric core/double-shell nanostructures.

In this paper, we aim to study the effect of shell permutation on the EM properties of core/double-shell nanostructures, featuring both conducting and insulating dielectric shells. Accordingly, two different core/double-shell nanostructured disks (i.e., $ZnFe_2O_4$/PANI/SiO_2 (ZPS) and $ZnFe_2O_4$/SiO_2/PANI (ZSP)) having a double-shell of PANI conducting dielectric and SiO_2 insulating dielectric coated on a disk-shaped $ZnFe_2O_4$ magnetic core are prepared, and their frequency-dependent electromagnetic properties are evaluated, together the $ZnFe_2O_4$ core. A special attention is put on the EM interaction at the core/1st shell and 1st shell/2nd shell interfaces.

ZPS and ZSP core/double-shell nanostructured disks were prepared using a surfactant-assisted hydrothermal method for the disk-shaped $ZnFe_2O_4$ core, a polymerization method for the PANI shell, and a modified stöber method for the SiO_2 shell. In a typical reaction for the $ZnFe_2O_4$ core, ZnAc of 2 mmol and $FeCl_3$ of 4 mmol were rapidly dissolved in distill water of 30 ml under stirring. When a transparent brown solution was formed, CTAB of 0.3 g and NaOH of 4 g were successively dispersed in the solution at a higher stirring speed. The resulting solution was transferred into a stainless steel autoclave of 50 ml with Teflon line before being heated in an oven at 200 °C for 4 h. After natural cooling, the $ZnFe_2O_4$ products were collected by a magnet and washed ultrasonically in absolute ethanol and water.

The double-shell coating sequence of PANI and SiO_2 depends on the designated shell permutation for ZPS and ZSP. The coating of the PANI shell was operated by a typical polymerization method.[9] The as-prepared $ZnFe_2O_4$ or SiO_2-coated $ZnFe_2O_4$ products were ultrasonically treated for 12 h in an aqueous solution of 120 ml containing polyvinylpyrrolidone of 10 g. After washed by ethanol and separated off, the magnetically collected $ZnFe_2O_4$ or SiO_2-coated $ZnFe_2O_4$ products were

[a]Author to whom correspondence should be addressed. Electronic mail: eeswor@polyu.edu.hk.

dispersed uniformly in a mixture of water of 50 ml, sodium dodecyl sulfate of 0.08 g, and aniline of 8 μl. Ammonium peroxodisulfate of 0.01 g was rapidly dropped into the mixture and kept stirring for 12 h. The coating of the SiO_2 shell was performed using a modified stöber method.[10] A modified reagent ratio at a reduced amount of NH_4OH catalyst was adopted to slow down the reaction for forming a thin and uniform SiO_2 layer. Accordingly, the $ZnFe_2O_4$ or PANI-coated $ZnFe_2O_4$ products were dispersed uniformly in a mixture of ethanol of 20 ml, water of 5 ml, and NH_4OH of 0.5 ml. Tetraethylorthosilicate of 0.2 ml was introduced in a drop-by-drop way under stirring. Then, stirring was maintained for an extended period of 20 h. For both shell-coating processes, the as-coated products were washed ultrasonically in absolute ethanol and water, separated magnetically, and dried in an oven at 40 °C.

The phase and crystallization of the products were examined by a Rigaku SmartLab X-ray diffractometer (XRD) with Cu-Kα radiation ($\lambda = 1.54$ Å) at a θ–2θ scan rate of 4°/min. The magnetization measurement was performed at room temperature using a LakeShore 7400 vibrating sample magnetometer. The morphology and nanostructure were investigated in a JEOL JEM-2100F transmission electron microscope (TEM), operating at 200 kV. The complex relative permittivity ($\varepsilon_r = \varepsilon_r' - j\varepsilon_r''$) and permeability ($\mu_r = \mu_r' - j\mu_r''$) of composite samples having 40 wt. % products dispersed in a paraffin matrix were measured by a transmission/reflection coaxial method in the 1–18 GHz range using an Agilent 5244A network analyzer. *RL* was determined using[8]

$$RL = 20\log|(Z_{in} - Z_0)/(Z_{in} + Z_0)|, \quad (1)$$

where $Z_{in} = Z_0(\mu_r/\varepsilon_r)^{1/2}\tanh[j(2\pi fd/c)(\mu_r\varepsilon_r)^{1/2}]$ is the input impedance of paraffin-bonded sample, $Z_0 \sim 377\ \Omega$ is the characteristic impedance of air, $c = 3 \times 10^8$ m/s is the velocity of light, and d is the thickness of paraffin-bonded sample.

Figure 1(a) shows the XRD θ–2θ pattern of a typical ZPS product. All peaks can be indexed to a pure $ZnFe_2O_4$ phase with space group of $Fd\bar{3}m$ according to JCPDS 22–1012. The slight increase in 2θ by 0.455° for all peaks infers a partially inverse spinel lattice in the $ZnFe_2O_4$ phase.[11] The extremely broad peak elevating the whole pattern from the background indicates an amorphous behavior of the PANI/SiO_2 double-shell. The magnetization hysteresis (*M*–*H*) loop in the inset reveals a ferromagnetic behavior with small coercivity of 17.8 Oe in the $ZnFe_2O_4$ core. It has been reported that $ZnFe_2O_4$ with a partially inverse spinel lattice exhibits ferromagnetism due to the partially inverted occupation of Zn^{2+} and Fe^{3+} in the *B* and *A* sites.[12] Figure 1(b) shows the TEM image of the ZPS product. Disk-shaped anisotropic morphology with a diameter of ~5 μm is seen. The SAED pattern in Fig. 1(c) contains diffraction spots and broad rings, suggesting a crystalline state of the disk-shaped $ZnFe_2O_4$ core as well as an amorphous state of the PANI/SiO_2 double-shell. Figure 1(d) illustrates the HRTEM image of the interfaces of the ZPS product. The periodic stripes of ~0.298 nm lattice plane spacing, corresponding to the (220) plane of $ZnFe_2O_4$, confirm the crystalline state of the disk-shaped $ZnFe_2O_4$ core. The two different layers with different contrasts grown on the $ZnFe_2O_4$ core are the amorphous PANI/SiO_2 double-shell. The 1st PANI shell is ~7 nm thickness when compared to the 2nd SiO_2 shell of ~19 nm (not shown). Figure 1(e) displays the HRTEM image of the interfaces of a typical ZSP product. A similar interfacial nanostructure to the ZPS product in Fig. 1(d) is observed. The 1st SiO_2 shell and the 2nd PANI shell are found to be ~5 and ~22 nm (not shown), respectively. The slight variations in the thickness of the two shells between the ZPS and ZSP products are mainly caused by the difference in growth mechanisms for coating the double-shells as well as the shrinking of PANI under the radiation of electron beam.

Figures 2(a) and 2(b) plot the frequency (f) dependence of the real (ε_r') and imaginary (ε_r'') parts of the complex relative permittivity (ε_r) of the paraffin-bonded $ZnFe_2O_4$, ZPS, and ZSP samples in the 1–18 GHz range, respectively. In Fig. 2(a), both ZPS and ZSP samples show similar quantitative reduction trends in ε_r' of ~20% when compared to the $ZnFe_2O_4$ sample in the whole measured f range. This is caused by disordered interfacial dipolar polarizations involving the insulating SiO_2 shell in the ZPS and ZSP samples. An extremely strong dielectric resonance is detected at 15.8 GHz in the ZPS sample due to the enhancement of interfacial dipolar polarization between $ZnFe_2O_4$ and PANI. In Fig. 2(b), both ZPS and ZSP samples show obvious reducing trends in ε_r'', with ~70% for the ZPS sample and a maximum of 40% for the ZSP sample, in comparison with the $ZnFe_2O_4$ sample. Besides, three dielectric resonances are observed for all samples, with the first two at 3.7 and 9.3 GHz being common to all samples. The third one is found to vary; that is, 15, 15.8, and 14.2 GHz for the $ZnFe_2O_4$, ZPS, and ZSP samples, respectively. For the ZPS sample, the extremely strong one at 15.8 GHz agrees with that found for ε_r' in Fig. 2(a). As electronic, ionic, and atomic polarizations are negligible at microwave frequencies, dipolar polarization should be the primary dielectric polarization for dielectric loss.[13] In order to study the effect of shell permutation on the dipolar polarization of the

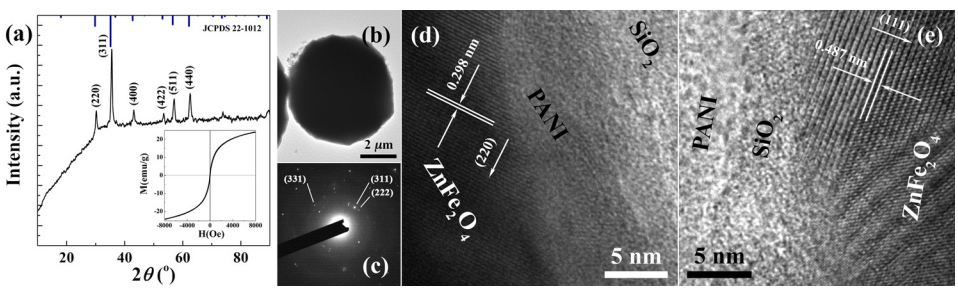

FIG. 1. (a) XRD θ–2θ pattern and *M*–*H* loop (the inset) of a typical ZPS product. (b) TEM image and (c) SAED pattern of ZPS product. (d) HRTEM image of the interfaces of ZPS product. (e) HRTEM image of the interfaces of a typical ZSP product.

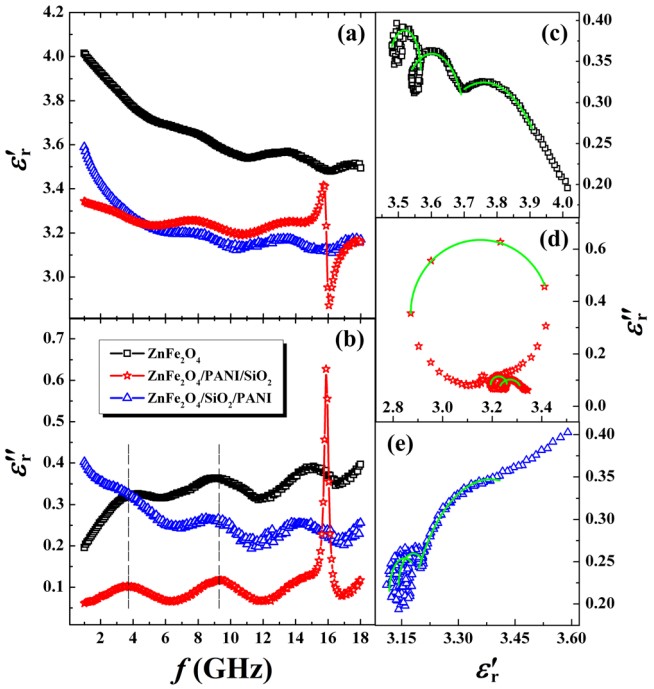

FIG. 2. f dependence of (a) ε_r' and (b) ε_r'' of ε_r of paraffin-bonded $ZnFe_2O_4$, ZPS, and ZSP samples. Cole-Cole plots and fitting semicircles for (c) $ZnFe_2O_4$, (d) ZPS, and (e) ZSP samples.

samples, Cole-Cole (i.e., ε_r'–ε_r'') plots for the $ZnFe_2O_4$, ZPS, and ZSP samples are produced in Figs. 2(c), 2(d), and 2(e), respectively, according to the Debye dipolar polarization theory described by[2]

$$(\varepsilon_r' - \varepsilon_\infty)^2 + (\varepsilon_r'')^2 = (\varepsilon_s - \varepsilon_\infty)^2, \quad (2)$$

where ε_∞ and ε_s are the optical dielectric constant and the stationary dielectric constant, respectively. Referring to Fig. 2(c) for the $ZnFe_2O_4$ sample, three obvious semicircles are clearly seen, reflecting the existence of triple Debye dipolar polarizations at 3.7, 9.3, and 14.8 GHz in it. For both ZPS and ZSP samples in Figs. 2(d) and 2(e), three semicircles, corresponding to the three dielectric resonances in Fig. 2(b), also exist, although the extremely strong one at 15.8 GHz results in a big semicircle, diminishing the other two at 3.7 and 9.3 GHz in the ZPS sample (Fig. 2(d)), while the two Debye dipolar polarizations at 9.3 and 14.2 GHz lead to two semicircles overlapping with each other in the ZSP sample (Fig. 2(e)). It is noted that the unchanged 1st and 2nd Debye dipolar polarizations at 3.7 and 9.3 GHz can be attributed to the intrinsic dipolar polarizations of the $ZnFe_2O_4$ sample, including the phase charge dipolar polarizations induced by lattice asymmetry and oxygen vacancies in the ferrite.[14] The 3rd Debye dipolar polarization, which varies with shell permutation at ~15 GHz, can be ascribed to the effect of interfacial dipolar polarization. For the $ZnFe_2O_4$ sample, the interfacial dipolar polarization should be generated by dipoles between the $ZnFe_2O_4$ molecules and the hydroxyl radicals. For the ZPS sample, the interfacial dipolar polarization at the PANI/SiO_2 interface is disordered by the insulating SiO_2 shell, so that it is induced by the difference in electronegativity between the $ZnFe_2O_4$ core and the conducting PANI shell instead and appears at a higher f of 15.8 GHz. For the ZSP sample, the interfacial dipolar polarizations at the $ZnFe_2O_4$/SiO_2 and SiO_2/PANI interfaces are both weakened, so that they shift to a lower f of 14.2 GHz. Considering a similar amount of dielectric polarizations, the increased amount of dipoles at the $ZnFe_2O_4$/PANI interface of the ZPS sample should result in a higher ε_r'' than the relatively less dipoles at the $ZnFe_2O_4$/SiO_2 and SiO_2/PANI interfaces of the ZSP sample. However, the ε_r'' spectra obtained in Fig. 2(b) present an opposite but interesting picture, which will be further explored in Fig. 3.

Figures 3(a) and 3(b) show the f dependence of real (μ_r') and imaginary (μ_r'') parts of the complex relative permeability (μ_r) of the paraffin-bonded $ZnFe_2O_4$, ZPS, and ZSP samples in the 1–18 GHz range, respectively. The $ZnFe_2O_4$ sample demonstrates the highest μ_r' and μ_r'' at the 1st magnetic resonance at 1.8 GHz, and then exhibits similarly decreasing trends with increasing f, except for the six subsequent magnetic resonances at 5, 7.2, 9.6, 11.3, 13.2, and 15.4 GHz. Among the four possible magnetic loss mechanisms: natural resonance, domain-wall displacement, hysteresis loss, and eddy-current loss,[3] the natural resonances induced by the magnetocrystalline anisotropy and exchange resonance should be the dominant magnetic loss contributor in the $ZnFe_2O_4$ sample. Domain-wall displacement may also have contribution as the size of our disk-shaped $ZnFe_2O_4$ cores (~5 μm) is larger than that of a single domain (<3 μm). Hysteresis loss can be neglected because the microwaves in our measurement were very weak. Eddy-current loss can also be neglected since the f dependence of $\mu_r''(\mu_r')^{-2}f^{-1}$, as shown in Fig. 3(c), is not a constant, and the skin-effect criterion cannot be fulfilled. Comparing to the $ZnFe_2O_4$ sample, both μ_r' and μ_r'' in the ZPS sample are significantly enhanced in the f ranges of 1.5–10.8 and 5.6–18 GHz,

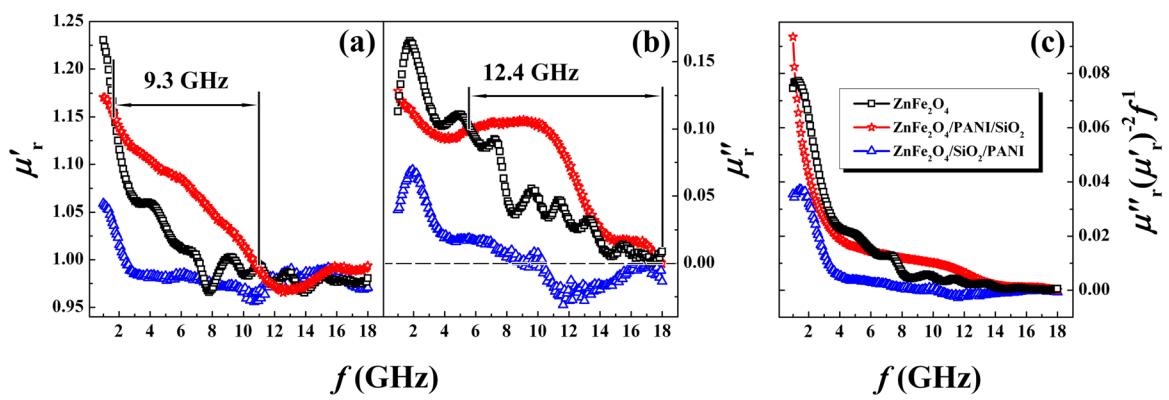

FIG. 3. f dependence of (a) μ_r' and (b) μ_r'' of μ_r of paraffin-bonded $ZnFe_2O_4$, ZPS, and ZSP samples. (c) f dependence of $\mu_r''(\mu_r')^{-2}f^{-1}$ for the samples.

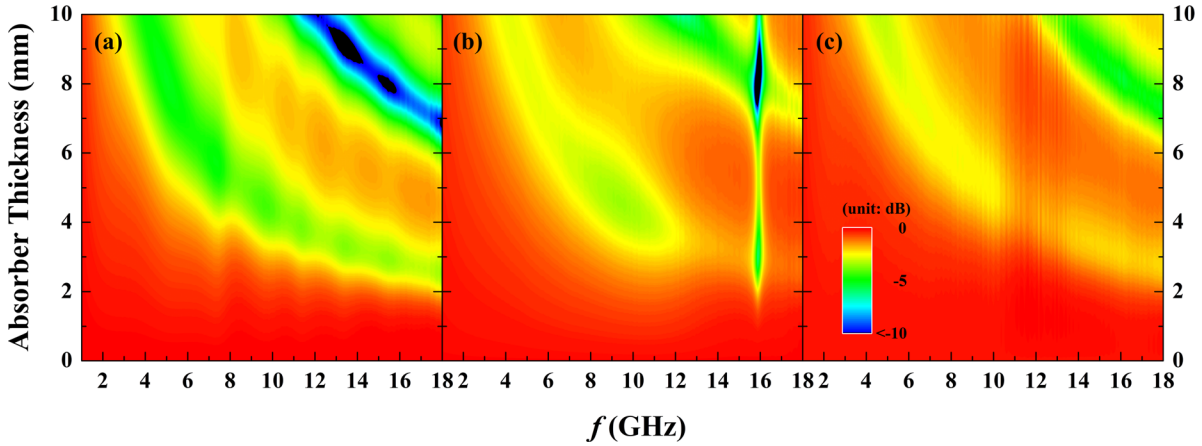

FIG. 4. 2*D*-contour plots of the dependence of *f* and *d* on *RL* for paraffin-bonded (a) $ZnFe_2O_4$, (b) ZPS, and (c) ZSP samples.

respectively. These cover the S and C bands of 9.3 GHz for μ_r' in Fig. 3(a) as well as the C, X, and Ku bands of 12.4 GHz for μ_r'' in Fig. 3(b). The fact that μ_r'' is significantly enhanced can be explained by the coating of conducting PANI shell on the magnetic $ZnFe_2O_4$ core to form a conducting coil as well as by further coating of insulating SiO_2 shell to insulate the conducting coil from the outside. Thus, the microwave magnetic fields will generate electric currents in the conducting PANI shell, leading to the transformation of magnetic energy into electric energy, corresponding to the increase in μ_r'' (magnetic loss) in Fig. 3(b) and the decrease in ε_r'' (dielectric loss) in Fig. 2(b). For the ZSP sample, both μ_r' and μ_r'' decline below the $ZnFe_2O_4$ and ZPS samples. Importantly, μ_r'' declines even below zero, and becomes negative in the 10–18 GHz range. Physically, a positive μ_r'' means magnetic loss, while a negative μ_r'' implies magnetic gain. Therefore, the decrease in μ_r'', especially the negative μ_r'', in Fig. 3(b) suggests the transformation of electric energy into magnetic energy through the generation of magnetic fields by the microwave electric currents. This, in turn, leads to an extra dielectric loss and increase ε_r'' in Fig. 2(b).[15] Although the insulating SiO_2 shell will weaken the dipolar polarization-related dielectric loss, the microwave electric currents in the conducting PANI shell will generate magnetic fields, thereby increasing ε_r'' in Fig. 2(b) as well as decreasing and forming negative μ_r'' in Fig. 3(b).

Figure 4 shows the 2*D*-contour plots of the dependence of *f* and absorber thickness (*d*) on *RL* for the paraffin-bonded $ZnFe_2O_4$, ZPS, and ZSP samples. For the $ZnFe_2O_4$ sample (Fig. 4(a)), *f* has a hyperbolic function of *d*, and strong absorption ($RL < -10$ dB) appears in the 12.6–14.3 and 15–15.8 GHz ranges for limited *d* ranges of 8.5–9.6 and 7.7–8.3 mm, respectively. By coating the double-shell, *RL* values are generally reduced in both ZPS and ZSP samples (Figs. 4(b) and 4(c)), with the reduction being less significant in the ZPS one. Interestingly, the ZPS sample shows a strong absorption ($RL < -10$ dB) in the 15.7–16.1 GHz range for an extended *d* range of 7.3–9.2 mm. This is a result of the extremely strong dielectric resonance at 15.8 GHz (Fig. 2). The higher absorption in the ZPS sample compared to the ZSP sample suggests an improved EM match enabled by the decrease in ε_r'' (dielectric loss) (Fig. 2(b)) and the increase in μ_r'' (magnetic loss) (Fig. 3(b)) through the magnetic-to-electric energy transformation.

We have prepared ZPS and ZSP core/double-shell nanostructured disks, and studied the effect of shell permutation on their EM properties, in conjunction with the $ZnFe_2O_4$ core. We have found the generally smaller ε_r' and ε_r'' in both ZPS and ZSP when compared to their parental core because of the presence of the insulating SiO_2 shell-induced disordered dipolar polarizations. Moreover, we have observed two obvious dielectric and magnetic abnormalities in ZPS and ZSP. They include (1) the weakening of ε_r'' in the dipolar polarization-rich ZPS, in comparison with the ZSP of relatively less dipolar polarization and (2) the enhancement of μ_r' and μ_r'' in the 1.5–10.8 and 5.6–18 GHz ranges, respectively, in ZPS, while the weakening of μ_r'' to negative in the 10–18 GHz range in ZSP, both when compared to the parental core. In addition, we have proposed an EM energy transformation mechanism to explain the observed abnormalities, thereby suggesting the transformation of magnetic energy into electric energy in ZPS through the generation of electric currents by the microwave magnetic fields, in contrast to the transformation of electric energy into magnetic energy in ZSP via the generation of magnetic fields by the microwave electric currents. This mechanism has been validated in absorption by providing an improved EM match between ε_r'' and μ_r'' in the ZPS sample when compared to the ZSP sample. The present study can provide useful information to developing magnetic/dielectric core/double-shell or core/multishell nanostructures.

This work was supported by the Research Grants Council of the HKSAR Government (PolyU 5236/12E) and The Hong Kong Polytechnic University (G-YK59).

[1]F. Qin *et al.*, J. Appl. Phys. **111**, 061301 (2012).
[2]X. Dong *et al.*, Appl. Phys. Lett. **92**, 013127 (2008).
[3]X. Zhang *et al.*, Appl. Phys. Lett. **89**, 053115 (2006).
[4]J. Zhu *et al.*, J. Phys. Chem. C **115**, 15304 (2011).
[5]X. Liu *et al.*, RSC Adv. **3**, 14590 (2013).
[6]X. Liu *et al.*, Mater. Res. Bull. **48**, 3887 (2013).
[7]X. Liu *et al.*, J. Alloy. Compd. **509**, 9071 (2011).
[8]X. Liu *et al.*, J. Appl. Phys. **115**, 17A507 (2014).
[9]C. Zhu *et al.*, Nanotechnology **18**, 275604 (2007).
[10]K. P. Velikov *et al.*, Appl. Phys. Lett. **80**, 49 (2002).
[11]J. Wu *et al.*, Appl. Phys. Lett. **99**, 202505 (2011).
[12]V. Blanco-Gutiérrez *et al.*, Chem. Mater. **22**, 6130 (2010).
[13]J. Tang *et al.*, Macromolecules **41**, 493 (2008).
[14]P. Nambissan *et al.*, J. Appl. Phys. **93**, 6320 (2003).
[15]X.-L. Shi *et al.*, Appl. Phys. Lett. **95**, 163108 (2009).